Materials and Design 195 (2020) 109017

Contents lists available at ScienceDirect

Materials and Design

journal homepage: www.elsevier.com/locate/matdes

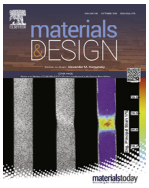

Enhanced mechanical properties in β-Ti alloy aged from recrystallized ultrafine β grains

Bingjie Zhang [a,b,*], Yan Chong [b], Ruixiao Zheng [b], Yu Bai [b], Reza Gholizadeh [b], Mingda Huang [a], Dong Wang [a], Qiaoyan Sun [a], Yunzhi Wang [a,d], Nobuhiro Tsuji [b,c,*]

[a] *Department of Materials Science and Engineering, Xi'an Jiaotong University, Xi'an, China*
[b] *Department of Materials Science and Engineering, Kyoto University, Kyoto, Japan*
[c] *Elements Strategy Initiative for Structural Materials (ESISM), Kyoto University, Kyoto, Japan*
[d] *Department of Materials Science and Engineering, The Ohio State University, Columbus, USA*

HIGHLIGHTS

- 480 nm grain size of recrystallized β structure could be obtained in β-Ti alloy for the first time.
- The ultrafine β structure made the precipitation structure of α finer and more uniform significantly.
- 1.6 GPa tensile strength and 9.1% total elongation could be achieved in the aged material having β grain size of 480 nm.
- Uniform precipitated structure supprressed crack initiation near β grain boundary.

GRAPHICAL ABSTRACT

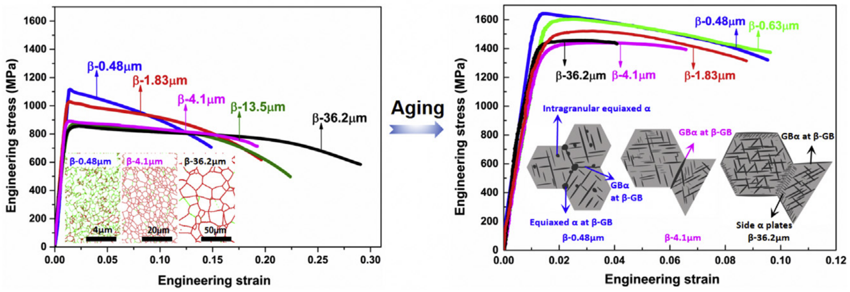

ARTICLE INFO

Article history:
Received 28 May 2020
Received in revised form 11 July 2020
Accepted 27 July 2020
Available online 30 July 2020

Keywords:
Ultrafine grain
α precipitation
Severe plastic deformation
Micro cracks
Fracture
Strength

ABSTRACT

Ultrafine β grain structures with recrystallized morphologies were fabricated by severe plastic deformation and subsequent annealing in Ti-10Mo-8 V-1Fe-3.5Al alloy. The minimum mean β grain size of 480 nm was obtained for the first time as a recrystallized structure in Ti alloys. Precipitation behavior of α in subsequent aging significantly changed with decreasing the recrystallized β grain size. Both tensile strength and total ductility of the aged Ti-alloy were increased by the β grain refinement. Tensile strength of 1.6 GPa and total elongation of 9.1% were achieved in the aged specimen having the prior β grain size of 480 nm, which was attributed to its finer and more homogeneous precipitated microstructure having a mixture of nanoscale thin-plate α and globular α without side α plates along β grain boundaries.

1. Introduction

Industrial applications of β-Ti alloys have attracted increasing attentions over recent years due to their capabilities to achieve various combinations of mechanical properties with precipitation-hardened microstructures [1]. Much attention has been paid to tune the size, spatial distribution, morphology of α precipitates for higher strength [2–5].

---

* Corresponding authors at Department of Materials Science and Engineering, Kyoto University, Kyoto, Japan.
E-mail addresses: bj3113305003@stu.xjtu.edu.cn (B. Zhang), nobuhiro-tsuji@mtl.kyoto-u.ac.jp (N. Tsuji).

https://doi.org/10.1016/j.matdes.2020.109017

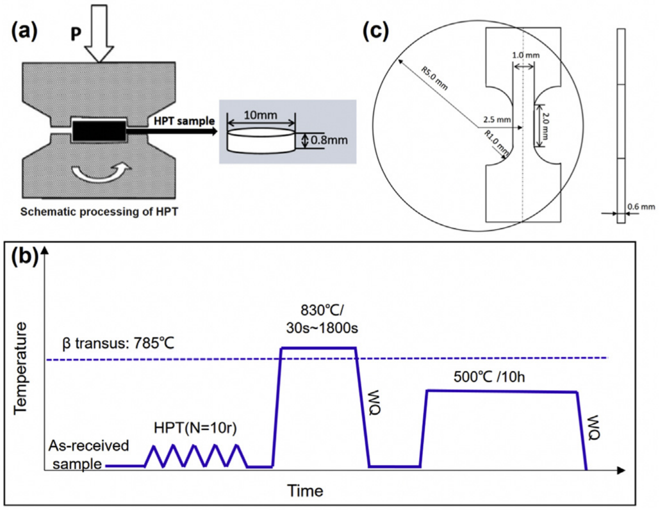

Fig. 1. (**a**) Schematic illustrations showing the HPT equipment and specimen used in the present study. P: compressive pressure of 6 GPa. (**b**) The whole processes for obtaining recrystallized and aged microstructures with different grain sizes in the Ti–10Mo-8 V-1Fe-3.5Al alloy. WQ: water quenching. (**c**) Schematic illustration showing the sampling location of tensile specimens.

However, the practical applications of β-Ti alloys have remained limited due to their poor ductility at strength levels above 1300 MPa, which is believed to be controlled not only by the precipitation behavior but by the prior β grain size (β-GS) as well [6,7]. Very recently, ultrafine β-grains with a mean GS below 50 nm have been attained by severe plastic deformation (SPD) in β-Ti alloys [7–10], like Ti-5Al-5 V-5Mo-3Cr (wt%) [11], Ti—20Mo (wt%) [12] and Ti—15Mo (wt%) [8]. However, the ultrafine grained (UFG) microstructures fabricated by SPD naturally have strain-hardened nature [13], so that they used to show limited tensile ductility both in β single phase state and after aging [14]. For overcoming this issue, it is necessary to realize ultrafine "recrystallized" structure of β phase [15]. The minimum recrystallized β-GS achieved by conventional plastic working and annealing has been about 10 μm, but in many cases the β-GS can easily coarsen to over 100 μm due to rapid diffusion in the β-phase that has a body-centered cubic structure [1,16–18]. This is likely to be the main reason why almost no investigations have reported ultrafine grained β in Ti alloys with recrystallized microstructures. It has been reported that metastable titanium alloys with relatively fine-grained (~10 μm) β-matrix in recrystallized state showed a rapid aging response, leading to optimized mechanical properties [6]. Thus, it is reasonable to consider that further refinement of the recrystallized β-GS down to a few micrometers or even below 1 μm would result in more unique α precipitation behavior, as well as good mechanical properties. The present study, therefore, firstly tries to refine the recrystallized β-GS of a metastable β-Ti alloy down to 1 μm. Their precipitation behaviors and resultant mechanical properties are also evaluated. Eventually, we show superior mechanical properties of the Ti alloy aged from the recrystallized UFG β-matrix.

2. Experimental procedure

A commercial metastable β-Ti alloy with a chemical composition of Ti-10Mo-8 V-1Fe-3.5Al (wt%) was used in this study. β-transus temperature of the alloy was estimated to be ~785 °C by differential scanning calorimetry. The as-received material was a rod of 10 mm in diameter forged at 830 °C and showed a hot-deformed microstructure of β single phase. Schematic illustrations of the high pressure torsion (HPT) process and specimen used in the present study are shown in Fig. 1 (**a**). Discs with a diameter of 10 mm and thickness of 0.8 mm for HPT were cut from the forged rods. HPT deformations up to 10 rotations ($N = 10\ r$) were conducted at room temperature at a speed of 0.5

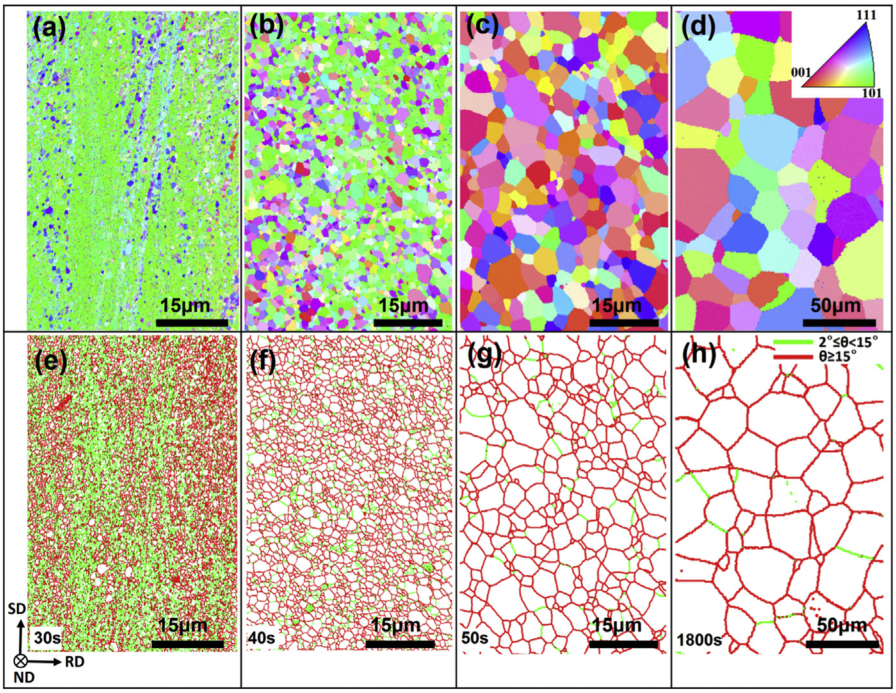

Fig. 2. EBSD maps of the specimens heavily deformed by HPT and then annealed for different periods at 830 °C. (**a-d**) Inverse pole figure (IPF) maps with different colors indicating crystallographic orientation parallel to the normal direction (ND) of the disc specimens according to the key stereographic triangle inserted in (**d**). (**e-f**) GB maps corresponding to (**a-d**) where high-angle boundaries (HABs) with misorientation angles $\theta \geqq 15^\circ$, and low-angle boundaries (LABs) with $2^\circ \leqq \theta < 15^\circ$ are drawn in red and green lines, respectively. The average grain sizes in these specimens are 0.48 μm (a,e), 1.83 μm (b, f), 4.1 μm (c, g) and 36.2 μm (d, h).

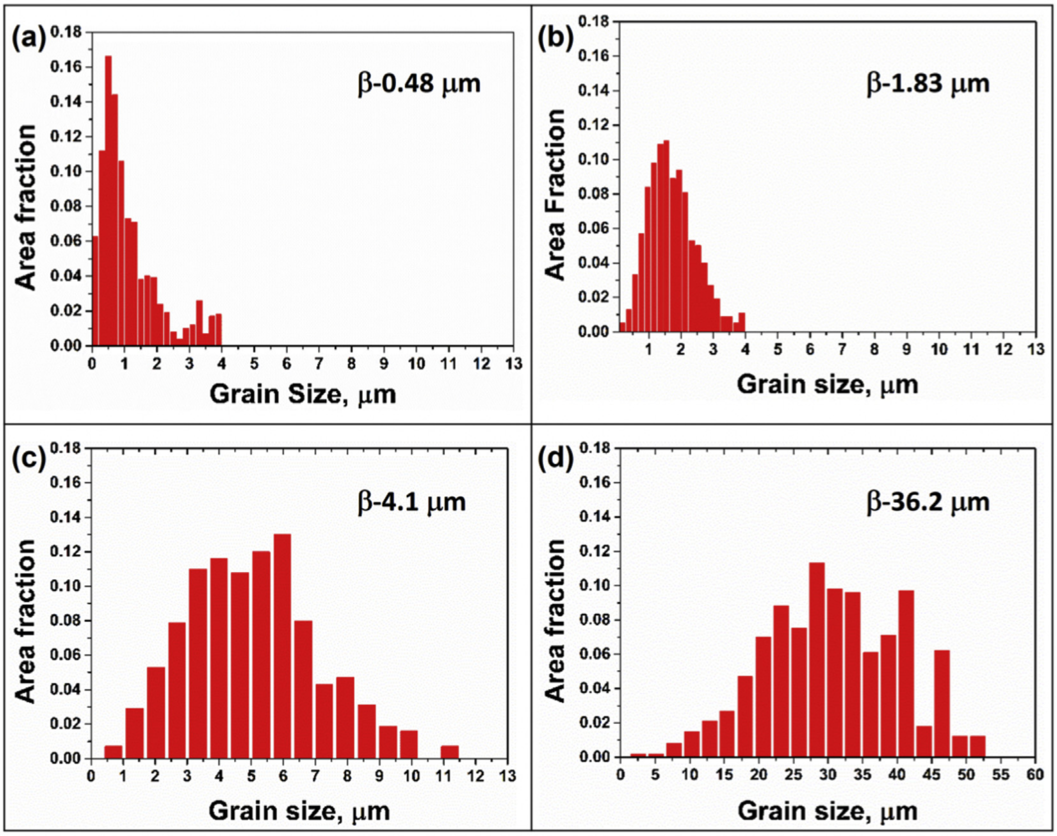

Fig. 3. Grain size distributions in the specimens with the mean grain sizes of **(a)** 0.48 μm, **(b)** 83 μm, **(c)** 4.1 μm, and **(d)** 36.2 μm.

revolution per minute under a compressive pressure (*P*) of 6.0 GPa. The HPT discs were subsequently annealed at 830 °C for 30 s, 40 s, 50 s or 1800 s followed by water quenching, and then the discs were aged at 500 °C for 10 h, as illustrated in Fig. 1 (**b**). All the heat treatments were carried out in a vacuum atmosphere to avoid oxidation. Microstructures were characterized by back-scattered electron (BSE) microscopy and electron backscattered diffraction (EBSD) using a scanning electron microscope equipped with a field emission gun (FE-SEM: JEOL 7100F). The microstructures were observed from the normal direction (ND) of the processed discs and at the position about 2.5 mm from its center. Electro-polishing of observed surfaces in a solution of 10% perchloric acid and 90% methanol at room temperature was conducted for EBSD measurements. High-Angle Annular Detector Dark-Field Scanning Transmission Electron Microscopy (HAADF-STEM) observations were performed using a transmission electron microscope (JEM-2100F). Thin-foil specimens for the transmission electron microscopy were prepared by a standard twin-jet electro-polishing technique using a Struers TenuPol-5 device. The as-processed discs 0.6 mm thick were firstly mechanically grounded from both sides of surfaces down to 40–50 μm in thickness. Disc slices 3 mm in diameter were then punched out from the thinned discs and then electro-polished in a solution of 5% perchloric acid, 35% N-butanol and 60% methanol at −40 °C at a voltage of 25 V. The microstructures were observed from ND of the processed discs and at the position about 2.5 mm from its center. X-ray diffraction (XRD) was conducted by the use of X'pert Pro equipment with an accelerated voltage of 40 kV and current of 40 mA. Nano-indentation mapping was performed on electro-polished surfaces of the specimens using a Hysitron Triboindenter system with a three-sided Berkovich indenter tip having a tip radius of 100 nm. Load-controlling indentation tests were done with a peak load of 500 μN and a holding time of 5 s. The distance between each indentation was set to be 800 nm for avoiding the effect of plastic deformation around the former indents. After the indentation, the location of each indentation was identified in the SEM-BSE image. Micro-tensile specimens with a gauge length of 2 mm, width of 1 mm and thickness of 0.6 mm were cut from the discs in such a way that the center of the gauge part coincided with the position at a distance of 2.5 mm from the center of the discs, as shown in Fig. 1 (**c**). Before tensile tests, the micro-tensile specimens were polished down to 0.35 mm thickness to remove surface layers. It has been confirmed in our previous studies [19–21] that the small-sized specimen can give reliable data of strength and tensile ductility equivalent to those obtained from standard-sized specimens of the same materials. Tensile tests were conducted on a Shimadzu AG-X plus system at an initial strain rate of 8.3×10^{-4} s^{-1}. Tensile strains of the micro-tensile specimens were precisely measured and analyzed by the digital image correlations (DIC) method with a Vic-2D commercial software. For each condition, three specimens were tested for confirming reproducibility and the average values were used to evaluate the tensile strength and ductility.

3. Results and discussions

3.1. Microstructures of Ti alloy with recrystallized UFG β grains

Fig. 2 shows EBSD maps of the specimens after HPT and subsequent annealing at 830 °C for different periods of time. All the specimens showed recrystallized microstructures of β single phase and the microstructures were fairly homogeneous in the observed areas. The microstructures were observed at the position about 2.5 mm from the center of the HPT processed discs. Fig. 2 **(a-d)** shows inverse pole figure (IPF) maps of the specimens annealed at 830 °C for 30 s, 40 s, 50 s, and 1800 s, respectively, where colors indicate crystallographic orientation parallel to the normal direction (ND) of the disc specimens according to the key stereographic triangle inserted in **(d)**. Fig. 2 **(e-h)** exhibits

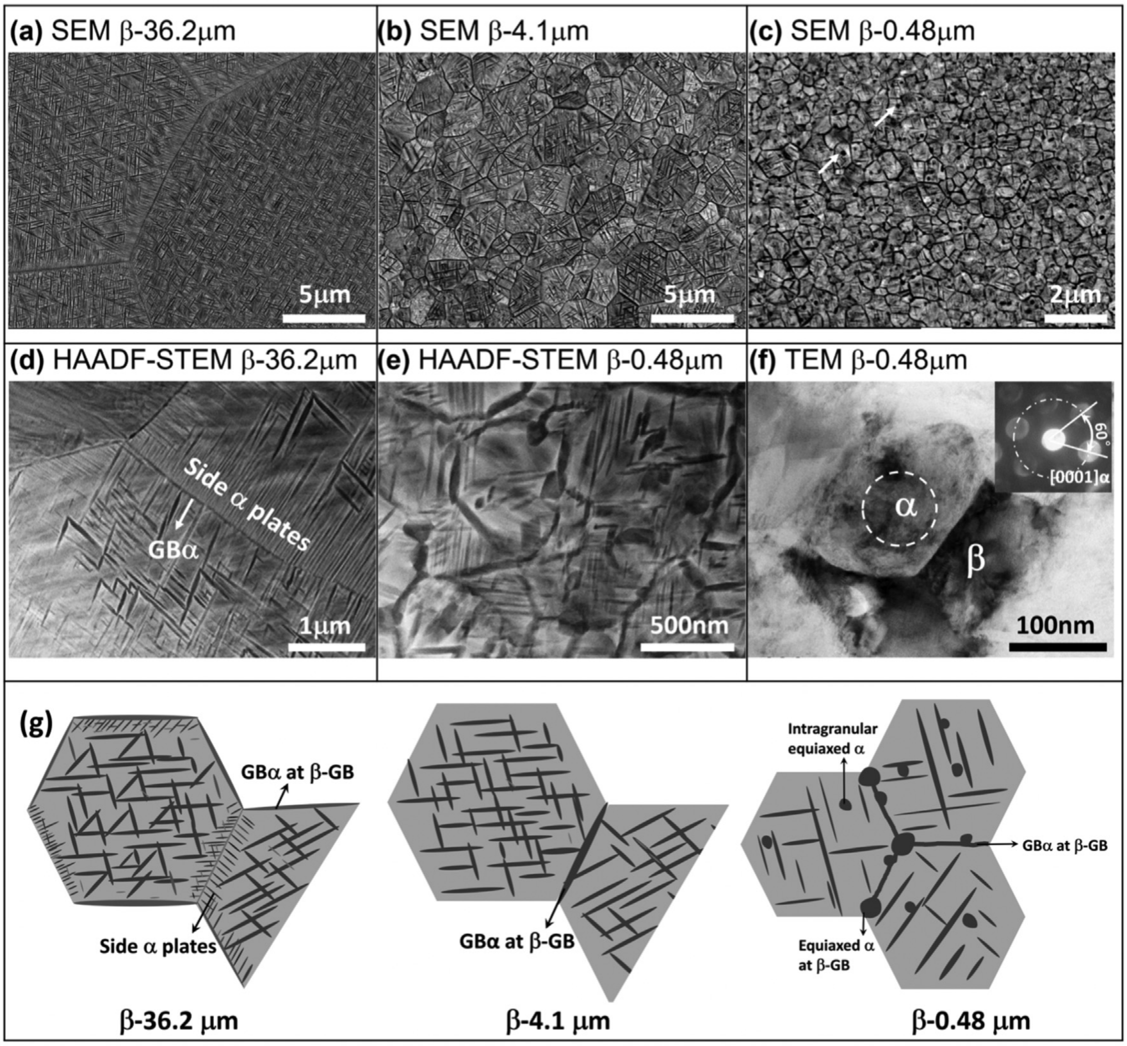

Fig. 4. Microstructures of the specimens HPT processed, annealed at 830 °C, and then aged at 500 °C for 10 h. Observed from ND of the discs. **(a, b, c)** SEM images of the aged microstructures with β-GSs of 36.2 μm, 4.1 μm and 0.48 μm, respectively. **(d, e)** HAADF-STEM images showing microstructures near β-GBs in the aged β-36.2 μm and β-0.48 μm specimens, respectively. **(f)** TEM image showing globularized α in the aged β-0.48 μm specimen, with a selected area diffraction pattern of the globularized α with the [0001] zone axis. **(g)** Schematic illustration showing the change of precipitation morphologies of α phase with decreasing the β grain size.

grain boundary (GB) maps corresponding to **(a-d)**, respectively. High-angle boundaries (HABs) with misorientation angles $\theta \geq 15°$, and low-angle boundaries (LABs) with $2° \leqq \theta < 15°$ are drawn in red and green lines, respectively, in the GB maps. The β-GS increased with increasing the annealing time at 830 °C and average β-GSs were measured as 0.48 μm (a, e), 1.83 μm (b, f), 4.1 μm (c, g) and 36.2 μm (d, h). The average grain sizes were measured by a line intercept method on EBSD GB maps of larger areas including a large number of grains enough for statistically reliable evaluation, counting both HAGBs and LAGBs. Grain size distributions in the specimen with different average grain sizes are shown in Fig. 3. In the specimen having the average grain size of 0.48 μm (Fig. **3** **(a)**), some grains had relatively large grain sizes of 3–4 μm, as was also recognized in Fig. 2 **(e)**. However, the number of coarse grains was quite limited and about 60% of grains had grain sizes smaller than 1 μm in the specimen having the mean grain size of 0.48 μm, as was also indicated in the grain size distribution (Fig. 3 **(a)**). The other specimens having larger average grain sizse showed fairly homogeneous (monomodal) grain size distributions, as shown in **Fig. 3** **(b)**, **(c)** and **(d)**. Hereafter, the corresponding specimens are referred to as the β-0.48 μm, β-1.83 μm, β-4.1 μm and β-36.2 μm specimens, respectively.

Such fine recrystallized β-GSs (0.48 μm and 1.83 μm) have not been reported previously in titanium alloys processed by conventional deformation and annealing. The EBSD IPF maps shown in Fig. 2 **(a-d)** indicated that the specimens having finer GSs (0.48 μm and 1.83 μm) showed a strong texture with 〈110〉 directions parallel to ND of the discs (green colors). On the other hand, the specimens with relatively coarse grain sizes (4.1 μm and 36.1 μm) showed nearly random texture. In the GB map of the ultrafine grained specimen (β-0.48 μm, Fig. 2 **(e)**), 49.1% of the observed boundaries were LABs. With increasing the annealing time (i.e., with increasing the average grain size), the fraction of LABs decreased, which corresponded to the change of the IPF maps (Fig. 2 **(a-d)**) with the grain growth. The green dominant colors in the β-0.48 μm specimen (Fig. 2 **(a)**) indicated a strong texture with {110} parallel to the disc surface (i.e., the shear plane in HPT), which was probably inherited from the shear texture formed by the HPT deformation where simple shear deformation along peripheral direction of discs was applied. In fact, EBSD analysis showed that the β-0.48 μm specimen had the strong (110)[001] texture, which is known as a typical component of shear textures in BCC metals and alloys. The large number of LABs in the β-0.48 μm specimen is attributed to this strong texture where many grains have similar orientation. With increasing the β

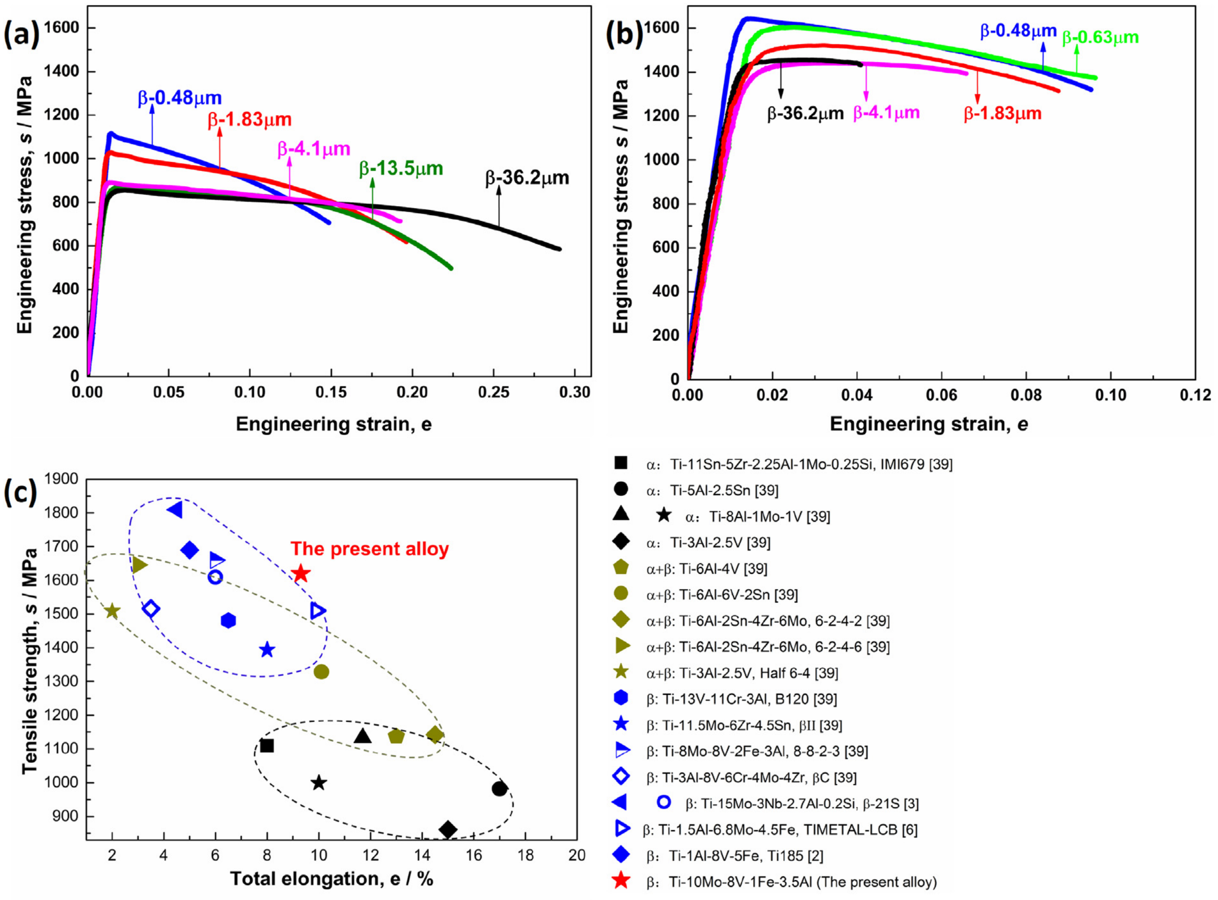

Fig. 5. Engineering stress-strain curves of **(a)** the specimens with β single-phase microstructures after HPT and annealing at 830 °C, and **(b)** the specimens with α + β dual phase microstructures after aging at 500 °C. **(c)** The strength-ductility balance in various kinds of Ti alloys. The black, dark yellow and blue symbols show tensile strength and total elongation previously reported in α-Ti alloys [39], α + β Ti alloys [39] and β-Ti alloys [2,3,6,39], respectively. The datum of the aged β-0.48 μm specimen obtained in the present study is indicated by a red star symbol.

grain size to 4.1 μm, fraction of green grain boundaries (LABs) decreased to 11% and grains with colors different from green increased in Fig. 2 **(b)**. Together with this change in grain orientations, the fraction of LABs in the β-0.48 μm specimen decreased, as shown in Fig. 2 **(f)**. When the grain growth progressed, grains had various colors (Fig. 2 **(c)** and **(d)**), and the fraction of LABs became very small (**Fig. 2** **(g)** and **(h)**). Although the tendency shown in **Fig. 2** that a strong shear-type texture in the UFG specimen weakened with the grain growth was confirmed, it was found that the texture components showed some variations depending on the observed locations in the disc specimens, probably due to the quite high plastic strains and the change of shear direction (i.e., the peripheral direction) in the HPT process. It was, therefore, difficult to confirm the detailed change of textures from the present data, which would be investigated in our future study.

Fig. 4 **(a)**, **(b)**, and **(c)** show SEM images of the β-36.2 μm, β-4.1 μm, and β-0.48 μm specimens, respectively, after aging at 500 °C for 10 h. Fig. 4 **(d)** and **(e)** are HAADF-STEM images of areas near β grain boundaries (β-GBs) in the aged β-36.2 μm and β-0.48 μm specimens, respectively. It could be seen that in the aged β-36.2 μm microstructure, high density of intragranular acicular α plates (57 ± 8 nm in thickness and 1348 ± 48 nm in length) with typical triangular morphologies were distributed homogeneously in interiors of β grains (Fig. 4 **(a)** and **(d)**). Along some β-GBs, many fine α plates precipitated in the same direction along β-GBs, which are known as "side α plates" (Fig. 4 **(d)**) [1]. The average width of the side α plates region was 1.98 ± 0.5 μm. With decreasing the β-GS to 4.1 μm (Fig. 4 **(b)**), the average thickness and length of intragranular α plates became 60 ± 10 nm and 911 ± 30 nm, respectively. The thickness of each α plate did not change, while the length clearly decreased with the refinement of β grains. It was noteworthy that side α plates were no longer observed. With further decreasing the β-GS to 0.48 μm (Fig. 4 **(c)** and **(e)**), the significant refinement of intragranular α, which was attributed to the decrease of volume of each β grain by the grain refinement, could be observed. Intragranular α had two different kinds of morphologies: one with a typical acicular shape of ~153 nm in length and ~ 36 nm in thickness, and the other with a globularized shape having an average diameter of 84 nm, as were pointed out by the white arrows in Fig. 4 **(c)** and recognized in **Fig. 4** **(e)**. It is noteworthy that both thickness and length of the acicular α plate decreased with decreasing the β grain size down to 0.48 μm. **Fig. 4** **(f)** is a TEM image showing a globularized α at β-GBs in the aged β-0.48 μm specimen. The selected area diffraction pattern with the zone axis of $[0001]_{\alpha}$ taken from the area indicated by the white-broken circle confirmed that the upper equiaxed grain in the micrograph was α phase. It was also confirmed from a diffraction pattern that the lower grain was a retained β phase having BCC structure. The globularized α were observed mostly on grain boundaries, especially at GB triple junctions. The change of precipitation morphologies of α phase with decreasing the β grain size is schematically illustrated in Fig. 4 **(g)**.

It was very interesting that the precipitation morphologies of α significantly changed with decreasing the grain size of β. It should be noted again that recrystallized β grains with grain sizes smaller than 2 μm have not been obtained in β-Ti alloys before the current study, so that it is also the first time to know such a change of α precipitation behavior. The number of studies on precipitation behavior from UFG mother phase with recrystallized morphologies is still quite limited even in any kinds of metallic alloys, and the mechanism of the morphology change of precipitates is unclear. However, the change of precipitation morphologies must be attributed to the significant increase of grain boundaries with grain refinement. Assuming that the GB area having disorders of atomic alignment compared to the periodical alignment inside grains is 1 nm, it can be calculated that the volume fraction of GB area increases from 0.0055% (a negligibly small value) to 0.11% or 0.42% by the grain refinement from 36.2 μm to 1.83 μm or 0.48 μm, respectively [22,23]. In β-Ti alloys, α phase nucleates preferentially at β-GBs forming grain boundary α (GB-α) with film shapes [24,25]. This is because GBs with higher free energies than the matrix can be preferential heterogeneous nucleation sites for α, and GBs and GB triple junction lines can act as fast diffusion paths. In the present study, GB-α was observed even in the UFG specimens naturally. The formation of globularized α at GB triple junctions in the β-0.48 μm specimen (Fig. 4 **(e, f)**) could be also understood from such advantages. Adjacent to the GB-α, side α plates formed in the specimen with coarse β grain size (β-36.2 μm), as was shown in Fig. 4 **(a)** and **(d)**. It is noteworthy that side α plates were no longer observed in the present study when the β-GS was smaller than 4.1 μm. It is known that side α plates are products of diffusional transformation appearing in certain kinds of Ti alloys at an early stage of aging at relatively low temperatures [26,27]. Similar to conventional α in Ti alloys, the side α plates maintain Burgers orientation relationship with β, but each side plate has very fine dimensions with thickness of 50 nm ~ 200 nm [28]. Qiu et al. [29–31] investigated the effects of grain boundaries on the morphology of grain boundary α (GB-α) and side α plates in Ti-6Al-4 V alloy by a three-dimensional phase field model. It was found that GB-α and side α plates compete with each other. Furuhara et al. [32] reported that side α plates showed a fast growth rate one-order higher than conventional α precipitates. As was shown above, the GB-α, a competitor of side α plates, preferentially formed also in the fine β grain specimens. Since distances between neighboring GBs decreases with decreasing the β grain size, diffusion fields in front of interfaces of growing α would overlap in tiny β grains, which might decrease the driving force for the precipitation of side α plates. Such a decrease of volumes of β grains as well as a decreased driving force for precipitation might explain the lack of side α plates and typical triangle morphologies of in-grain α plates.

It has been reported that elongated GB α films are preferential paths of crack propagation [33]. This is probably because the elongated GB α having the same crystallographic orientation plays a role of coarse and relatively hard domain to induce stress concentrations at interfaces. Having globularized α in the middle of elongated GB α is believed to obstruct crack propagation during deformation [1,34]. For increasing the resistance to microcrack propagation, hot-deformations were industrially applied to change the GB-α to globularized α with grain sizes of several microns [1]. In the current study, diameters of the globularized α formed from the ultrafine grained β were less than 100 nm (Fig. 4 **(e)**). The significant refinement of α phase (both acicular α plates inside β-grains and globularized α) in the β-0.48 μm specimen is expected to be beneficial for mechanical properties, which will be discussed later.

3.2. Mechanical properties of the specimens with different β-GSs

Engineering stress-strain curves of the specimens with single β phase microstructures (after annealing) and α + β two-phase microstructures (after aging) are shown in Fig. 5 **(a)** and **(b)**, respectively. In Fig. 5 **(a)**, all the β single-phase specimens having different β-GSs showed similar shapes of stress-strain curves. The flow stress reached their maximum at early stages of deformation, so that the uniform elongation of the specimens was limited. However, the flow stress slowly decreased even after the peak stress, leading to a large post-uniform elongation and a total elongation over 15% for all the specimens. These are typical shapes of stress-strain curves of highly-alloyed β-Ti alloys. The β-36.2 μm specimen showed a typical tensile properties of such β-Ti alloys with a tensile strength of 856 ± 11 MPa and a large total elongation of 29 ± 3%, but strain hardening after yielding was limited to show a small uniform elongation of 3.3%. Such a tensile behavior in β-Ti alloys is probably due to high yield strength owing to solution hardening by large amounts of alloying elements included in the alloy and essentially suppressed strain-hardening ability in BCC crystal. In such highly-alloyed β-Ti alloys having stable BCC β phase, it is difficult to induce other deformation mechanisms for increasing strain hardening, such as martensitic transformation and deformation twinning [35–37] even in coarse β-grained specimens. The strength did not increase when the β-GS was reduced to 4.1 μm, while a significant increase of strength was observed when the β-GS decreased below 1.83 μm. The β-0.48 μm specimen exhibited the tensile strength of 1116 ± 15 MPa and a total elongation of 15 ± 2%. Considering the original mechanical property of the coarse-grained (β-36.2 μm) specimen described above, it is understandable that the β-0.48 μm specimen exhibits low tensile ductility without strain hardening after yielding at high stress, which is also typical in nanostructured alloys [38].

After aging (Fig. 5 **(b)**), the tensile strength of the aged β-36.2 μm specimen increased to 1450 ± 14 MPa with a total elongation of 4.5 ± 0.8%. Similar to the strength of the β single-phase specimens, the strength exhibited almost no enhancement till the β-GS decreased to 4.1 μm, although the ductility of the β-4.1 μm specimen increased to 6.6 ± 1%. When the β-GS was further refined to a sub-micrometer scale, strength of the specimens increased with the refinement of the β-GS. The β-0.48 μm specimen showed a tensile strength of 1603 ± 54 MPa. Volume fractions of α phase in the β-0.48 μm, β-4.1 μm and β-36.2 μm specimens were evaluated as 47.1%, 44.2% and 46.5%, respectively, by Rietveld analysis of XRD results for the specimens. The result indicated that the refinement of β-grains down to 0.48 μm grain size had no influence on the volume fraction of α. It can be concluded that α phase reached the equilibrium volume fraction after a long time (10*h*) aging at 500 °C in all specimens with different β grain sizes [1]. Nevertheless, both the length and thickness of the acicular α has significant refinement (from ~60 nm to 36 nm in thickness, and from 1348 nm to 153 nm in length) with decreasing the β-GS from 36.2 μm to 0.48 μm. This significant ultra-refinement of α must contribute to strengthen the alloy, as many previous investigations on β-Ti alloys reported [1,3,6]. Measured yield strength (0.2% proof stress) of the

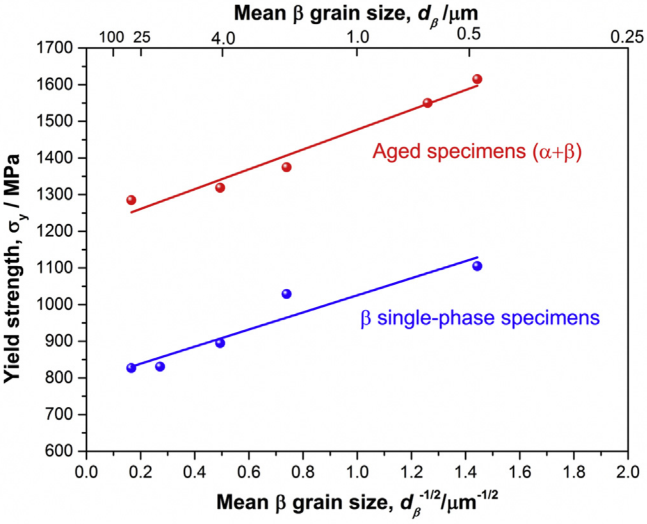

Fig. 6. Yield strength (0.2% proof stress) of the specimens having β single-phase microstructures (before aging) or α + β microstructures (after aging) are plotted as a function of the minus square root of the mean β grain sizes.

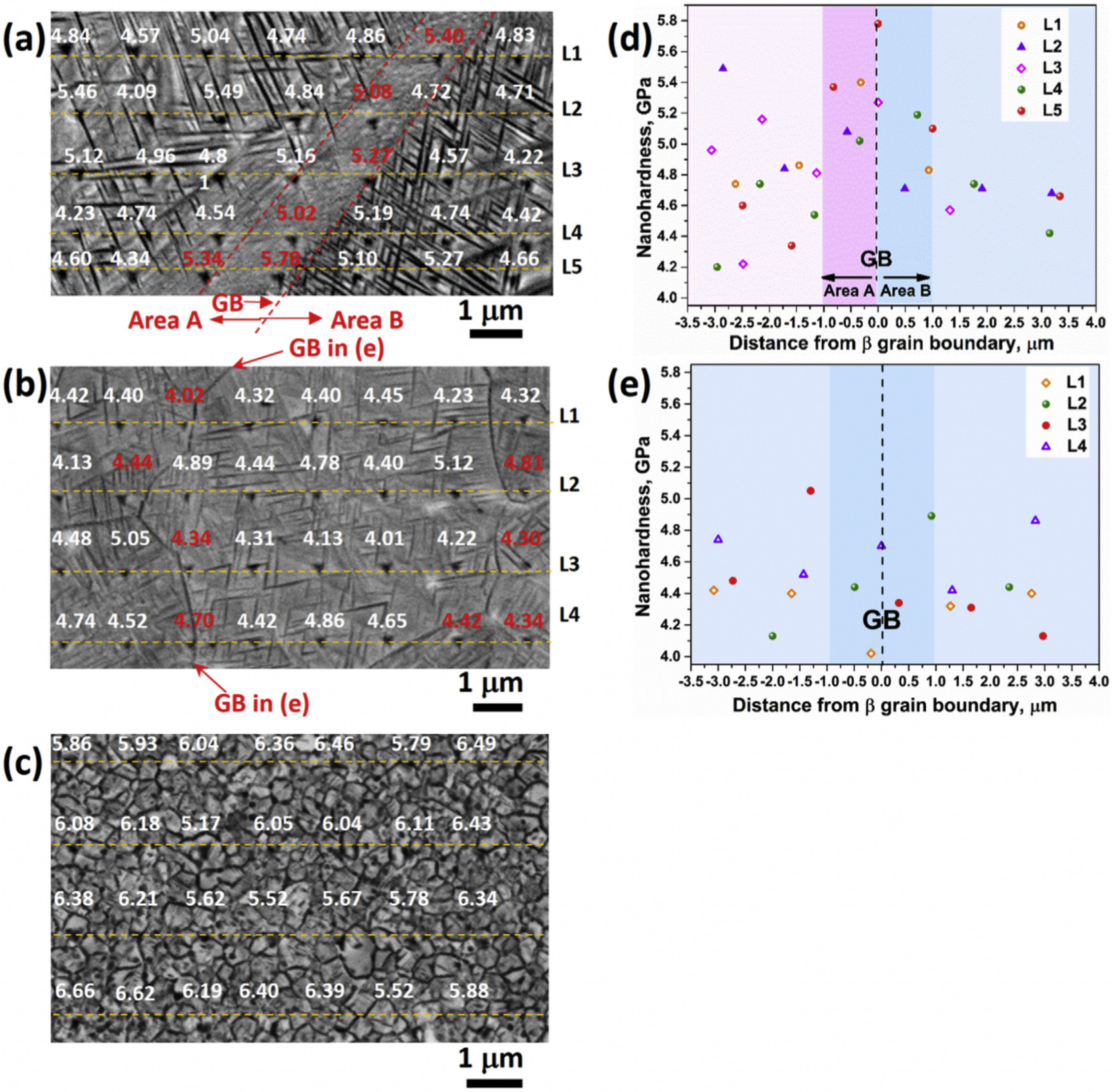

Fig. 7. Experimental results of nano-indentation mapping for the aged specimens with different prior-β grain sizes. (**a**) SEM image around a β-GB with side α plates together with the values of nanohardness at different positions of the aged β-36.2 μm specimen. The nanohardness values near the β-GB are shown in red. (**b**) SEM image together with the values of nanohardness at different positions of the aged β-4.1 μm specimen. The nanohardness values near β-GBs are shown in red. (**c**) SEM image together with the values of nanohardness at different positions of the aged β-0.48 μm specimen. (**d**) Nanohardness values along different measurement lines (L1 ~ L5) across the β-GB in (a), plotted as a function of the distance from the β-GB in the aged β-36.2 μm specimen. (**e**) Nanohardness values along different measurement lines (L1 ~ L4) across the β-GBs in (b), plotted as a function of the distance from the β-GBs in the aged β-4.1 μm specimen.

specimens having β single-phase microstructures (before aging) or α + β microstructures (after aging) are plotted as a function of the minus square root of the mean β grain sizes in Fig. 6. The yield strength of both types of specimens showed linear increases with the β grain refinement in Fig. 6, which indicated that Hall-Petch relationship stood. It is understandable that the yield strength of the specimens having β single-phase microstructures shows a Hall-Petch relationship. On the other hand, it is interesting that the specimens with α + β microstructures also holds a Hall-Petch relationship with the grain size of β, since their microstructures are composed of two different phases, i.e., finely divided retained β phase and fine α phase with different morphologies. In such fine and complicated microstructures, dislocation slips would be inhibited in various ways. At this moment, therefore, it is difficult to quantitatively explain the strengthening of the aged specimens with decreasing the grain size of prior β grains, but we may qualitatively summarize that the refinement and the change of morphologies of α precipitates result in the significant strengthening of the alloy.

It is concluded from the results by now that the refinement of β-GS below ~2 μm can significantly enhance the strength of the alloy both before and after aging, although the grain refinement down to ~4 μm does not change the strength so much. It is interesting that the tensile elongation (total elongation) of the aged specimens rather increased when the β-GS decreased down to sub-micrometers (Fig. 5 (**b**)). The total elongation of the β-0.48 μm specimen was 9.1%. The aged specimens did not show large uniform elongation, but it was a general feature of the precipitation-hardened metallic alloys which primarily required high yield strength. Even for such precipitation-hardened alloys, it is beneficial that the total elongation increased with ultra-grain refinement in the present high-strength β-Ti alloy, for increasing toughness to avoid catastrophic fracture. Fig. 5 (**c**) shows the strength-ductility balance in various kinds of Ti-alloys. The aged β-0.48 μm specimen obtained in this study exhibited one of the best strength-ductility balances among the data, especially in high strength regions of tensile strength above 1500 MPa. It can be, therefore, concluded that the refinement of

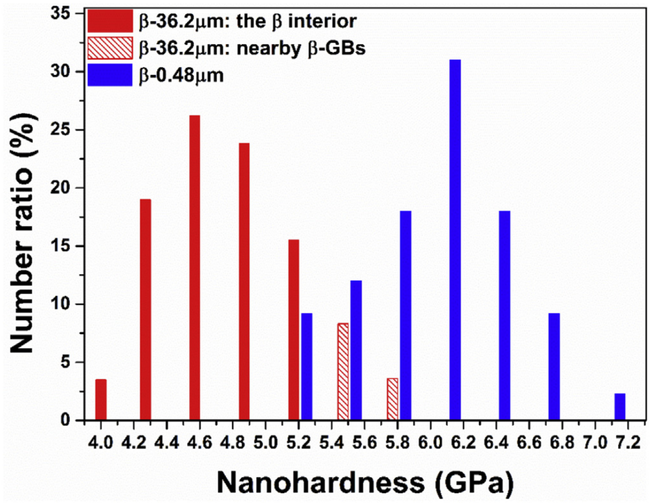

Fig. 8. Number ratio of nanohardness values in the aged β-36.2 μm and β-0.48 μm specimens.

β-GS, especially below 1 μm, in the recrystallized state is beneficial for realizing superior mechanical properties in β-Ti alloys.

3.3. Fracture analysis of the aged specimens with different β-GSs

The increase in strength in the present specimens having ultrafine recrystallized β-GS is attributed to the significant refinement of both prior β-grains and α-precipitates shown in **Figs. 2, 3** and **4**. It is noteworthy that the ductility of the aged specimens rather increased with decreasing the β-GS below 2 μm (Fig. 5 (**b**)). In order to clarify the reason why the ductility of the aged specimens having higher strength increased with decreasing the β-GS, nano-indentation analysis were carried out in the aged specimens with β-GSs of 36.2 μm, 4.1 μm and 0.48 μm, respectively, and obtained results are shown in Fig. 7. **Fig. 7** (**a**) shows the distribution of nanohardness values near a β-GB in the aged β-36.2 μm specimen. As was shown in Fig. 4 (**a**) and (**d**), this specimen showed typical side α plates along β-GBs. Fig. 7 (**a**) is an SEM image around such a β-GB with side α plates, together with the values of nanohardness at different positions. The nanohardness values near the β-GB are shown in red. The side α plates could be recognized as a white band in the SEM image, which showed a morphology different from that of the typical acicular α plates with triangle morphologies in interiors of β grains. It should be noted that the nanohardness values within the side α plate regions (average 5.31 ± 0.21 GPa) were significantly higher than those in the intragranular α-plate regions (average 4.78 ± 0.39 GPa). These nanohardness values along lines across the β-GB are plotted as a function of the distance from the β-GB in Fig. 7 (**d**).

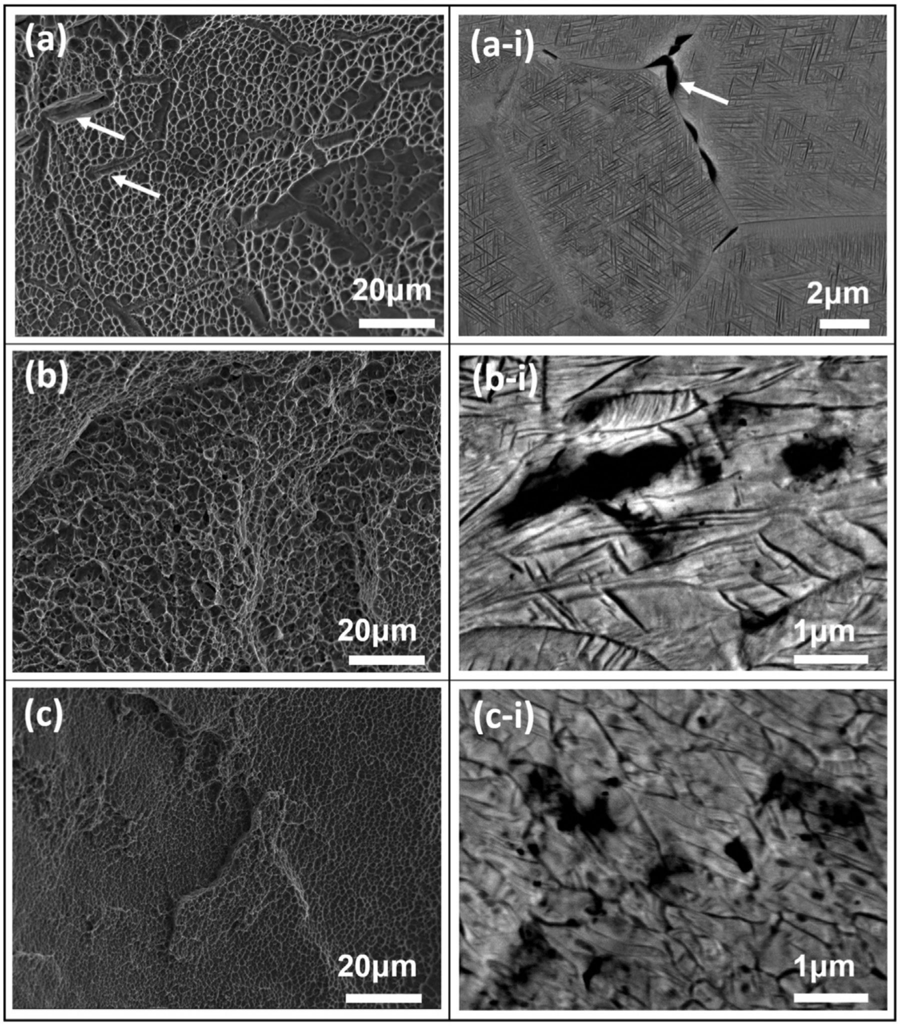

Fig. 9. SEM images of fracture surfaces of the aged specimens with the β-GS of (**a**) 36.2 μm, (**b**) 4.1 μm and (**c**) 0.48 μm. SEM images showing micro-cracks initiated in microstructures of the aged specimens with the β-GS of (**a-i**) 36.2 μm, (**b-i**) 4.1 μm and (**c-i**) 0.48 μm.

From this graph, the increase of nanohardness with approaching to the β-GB was obviously recognized. Fig. 7 **(b)** is an SEM image together with the nanohardness values at different positions in the aged β-4.1 μm specimen. The nanohardness values near β-GBs are shown in red again. The hardness values are plotted in Fig. 7 **(e)**, as a function of the distance from the left β-GB marked by the red arrows in Fig. 7 **(b)**. In this specimen, no side α plates were observed near β-GBs (Fig. 4 **(b)**). Although the hardness fluctuated depending on the position, nanohardness values near the β-GBs (red values in Fig. 7 **(b)**; average 4.61 ± 0.45 GPa) were not so much higher than those in β interiors (white values in **Fig. 7 (b);** average 4.51 ± 0.27 GPa), which was also confirmed in **Fig. 7** **(e)**. **Fig. 7** **(c)** is an SEM image together with the values of nanohardness at different positions in the aged β-0.48 μm specimen. In this case, the values of nanohardness was rather uniform, but the average value was 6.13 ± 0.35 GPa which was much higher than the nanohardness in the specimens having the average b grain size of 36.2 μm and 4.1 μm.

Fig. 8 shows number ratios of the nanohardness values in the aged β-36.2 μm and β-0.48 μm specimens. The hardness values in the β-0.48 μm specimen in Fig. 8 were much higher than those in the β-36.2 μm specimen, which corresponded to the higher strength obtained from the tensile tests (Fig. 5 **(b)**). The higher hardness values within the β-36.2 μm specimen were all obtained within the side α plate regions near β-GBs. Difference in local hardness (strength) in microstructures of precipitation-hardening alloys is considered to lead to a difference in plastic strains between adjacent local regions with different hardness, causing incompatibilities in deformation, initiation of cracks between domains, and a decrease in tensile ductility [33].

Fig. 9 **(a)**, **(b)** and **(c)** are SEM micrographs of fracture surfaces of the aged specimens with different β-GSs, while Fig. 9 **(a-i)**, **(b-i)** and **(c-i)** are SEM images showing micro-cracks observed near main cracks in these aged specimens. As was indicated by the white arrows in Fig. 9 **(a)** of the aged β-36.2 μm specimen, some areas showed brittle-like fracture surfaces with flat morphologies. Such fracture surfaces had characteristic elongated morphologies, which seemed to correspond to β-GBs. Microcracks in the aged β-36.2 μm specimen shown in Fig. 9 **(a-i)** clearly indicated that voids and cracks were initiated near β-GBs with white banded regions, i.e., side α plates. This result demonstrates that the strength (hardness) difference between the side α plate regions and the β grain interiors (shown in Fig. 7) initiated microcracks at β-GBs with the side α plates. No side α plate regions were observed in the aged β-4.1 μm and β-0.48 μm specimens as was shown in Fig. 4 **(b, c, e)**, and fracture surfaces were homogeneous and showed only ductile fracture characteristics with dimples (Fig. 9 **(b)**, **(c)**). This indicated that the disappearance of side α plates inhibited the initiation of brittle fracture along β GBs in the specimens having fine β grain sizes The size of dimples in the aged β-0.48 μm specimen was much finer than that in the aged β-4.1 μm specimen. Microvoids in the aged β-4.1 μm and β-0.48 μm specimens were nucleated mostly inside the prior β-grains (Fig. 9 **(b-i), (c-i)**), which coincided with the suppression of brittle fracture along prior β GBs.

It can be concluded, therefore, that the ultra-refinement of recrystallized β-grains makes the final α + β microstructures finer and more homogeneous (a mixture of fine acicular and globular α without side α plates near β-GBs), avoiding deformation incompatibilities between different domains and brittle crack initiation to result in the larger tensile ductility. Refinement of α precipitates in UFG β grains was also beneficial for increasing strength of the aged specimens. Ultra-refinement of β grains with recrystallized morphologies are beneficial for both high strength and adequate ductility in the age-hardened β-Ti alloys.

4. Conclusions

We tried to make ultrafine grained β phase with recrystallized morphologies in a Ti-10Mo-8 V-1Fe-3.5Al (wt%) alloy, and succeeded in the grain refinement. The obtained recrystallized ultrafine β specimens were subsequently aged, and mechanical properties of the specimens before and after aging were systematically investigated. The major results obtained in the present study are as follows.

(1) The β grain refinement below 1 μm in the recrystallized state was achieved for the first time in a β-Ti alloy using heavy deformation by HPT at ambient temperature followed by annealing under appropriate conditions. The minimum β-GS obtained was 0.48 μm (480 nm), which is the minimum recrystallized grain size of β in Ti alloys. Ultra-refinement of the recrystallized β grain size led to unique precipitation behavior during subsequent aging.
(2) With reducing the β grain size to 4.1 μm, the sizes and morphologies of α precipitates in β grain interiors as well as near β grain boundaries significantly changed, compared to those in the coarse grained β-36.2 μm specimen. Side α plates no longer formed below 4.1 μm of the β grain size. The change in sizes and morphologies of α precipitates led to more homogeneous precipitated microstructures than those formed from coarse β structures.
(3) The yield strength of the β single-phase specimens increased with decreasing the recrystallized β grain size, keeping the total elongation over 15%, although the uniform elongation of the all β single-phase specimens was limited regardless of the β grain size. Strength of the aged specimen was significantly enhanced when the β grain size became finer than about 2 μm. It was noteworthy that the total elongation of the aged specimens increased with decreasing the β grain size. The aged β-0.48 μm specimen having finer α precipitates exhibited the high tensile strength of 1603 MPa and the total elongation of 9.1%, while those of the aged β-36.2 μm specimen were 1450 MPa and 4.5%, respectively.
(4) The side α plate regions near β grain boundaries showed higher hardness than other regions in the β-36.2 μm specimen, which caused the initiation of microcracks near β grain boundaries due to deformation incompatibility between the side α plate regions and grain interiors. The ultra-refinement of recrystallized β-grains makes the final α + β microstructures finer and more homogeneous (a mixture of fine acicular and globular α without side α plates near β-GBs), avoiding deformation incompatibilities between domains and brittle crack initiation to result in the larger tensile ductility. It is concluded from the present results that ultrafine grained β microstructures with recrystallized morphologies are beneficial for both high strength and adequate ductility in the age-hardened β-Ti alloys, through making the precipitation microstructures finer and more homogeneous.

CRediT authorship contribution statement

Bingjie Zhang: Conceptualization, Methodology, Investigation, Writing-original draft, Writing-review & editing. **Yan Chong:** Investigation, Writing-review & editing. **Ruixiao Zheng:** Investigation, Writing-review. **Yu Bai:** Investigation. **Reza Gholizadeh**: Crystallographic analysis. **Mingda Huang:** Investigation. **Dong Wang:** Writing-review. **Qiaoyan Sun:** Writing–review. **Yunzhi Wang:** Writing-review & editing, Project administration. **Nobuhiro Tsuji:** Conceptualization, Methodology, Investigation, Writing-original draft, Writing-review & editing, Supervision, Project administration.

Data availability

The data that support the findings of this study are available from the corresponding authors upon reasonable request.

Declaration of Competing Interest

The authors declare that they have no known competing financial interests or personal relationships that could have appeared to influence the work reported in this paper.

Acknowledgement

This study was supported by the Cross-Ministerial Strategic Innovation Promotion Program on Structural Materials for Innovation (SIP-SMI), Japan, the Elements Strategy Initiative for Structural Materials (ESISM) in Kyoto University (No. JPMXP0112101000), Japan, the Grant-in-Aid for Scientific Research (S) (No. 15H05767), the Grant-in-Aid for Scientific Research (A) (No. 20H00306), JST CREST (No. JPMJCR1994), the National Key Research and Development Program of China (Grants No. 2016YFB0701302 and No. 2014CB644003), and the National Natural Science Foundation of China (Grants No. 51671156, 51671158). The authors wish to thank the Northwest Institute for Non-ferrous Metal Research of China for the supply of the material.

References

[1] G. Lütjering, J.C. Williams, Titanium, second ed. Springer, Berlin, 2007.

[2] A. Devaraj, V.V. Joshi, A. Srivastava, S. Manandhar, et al., A low-cost hierarchical nanostructured beta-titanium alloy with high strength, Nat. Commun. 7 (2016) 1–8.

[3] S.A. Mantri, D. Choudhuri, T. Alam, et al., Tuning the scale of α precipitates in β-titanium alloys for achieving high strength, Scr. Mater. 154 (2018) 139–144.

[4] B. Jiang, S. Emura, K. Tsuchiya, Improvement of ductility in Ti-5Al-5Mo-5V-3Cr alloy by network-like precipitation of blocky α phase, Mater. Sci. Eng. A 722 (2018) 129–135.

[5] A. Boyne, D. Wang, R.P. Shi, et al., Pseudospinodal mechanism for fine α/β microstructures in β-Ti alloys, Acta Mater. 64 (2014) 188–197.

[6] O.M. Ivasishin, P.E. Markovsky, S.L. Semiatin, et al., Aging response of coarse- and fine-grained β titanium alloys, Mater. Sci. Eng. A 405 (2005) 296–305.

[7] I.P. Semenova, V.V. Polyakova, G.S. Dyakonov, et al., Ultrafine-grained titanium-based alloys: structure and service properties for engineering applications, Adv. Eng. Mater. 22 (2019) 1.

[8] K. Václavová, J. Stráský, I. Semenova, et al., Microhardness and microstructure evolution of ultra-fine grained Ti-15Mo and TIMETAL LCB alloys prepared by high pressure torsion, Mater. Sci. Eng. A 682 (2017) 220–228.

[9] K.Y. Xie, Y. Wang, R.Z. Valiev, et al., Nanocrystalline β-Ti alloy with high hardness, low Young's modulus and excellent in vitro biocompatibility for biomedical applications, Mater. Sci. Eng. C 33 (2013) 3530–3536.

[10] I.P. Semenova, E.B. Yakushina, V.V. Nurgaleeva, et al., Nanostructuring of Ti-alloys by SPD processing to achieve superior fatigue properties, Int. J. Mater. Res. 100 (2009) 1691–1696.

[11] A. Zafari, X.S. Wei, W. Xu, et al., Formation of nanocrystalline β structure in metastable beta Ti alloy during high pressure torsion: the role played by stress induced martensitic transformation, Acta Mater. 97 (2015) 146–155.

[12] W. Xu, X. Wu, M. Stoica, et al., On the formation of an ultrafine-duplex structure facilitated by severe shear deformation in a Ti–20Mo β-type titanium alloy, Acta Mater. 60 (2012) 5067–5078.

[13] J.A. Benito, R. Tejedor, R. Rodríguez-Baracaldo, et al., Ductility of bulk nanocrystalline and ultrafine grain iron and steel, Mater. Sci. Forum 633-634 (2010) 197–203.

[14] K. Sharman, P. Bazarnik, T. Brynk, et al., Enhancement in mechanical properties of a β-titanium alloy by high-pressure torsion, J. Mater. Res. Technol 4 (2015) 79–83.

[15] N. Tsuji, R. Gholizadeh, R. Ueji, et al., Formation mechanism of ultrafine grained microstructures: various possibilities for fabricating bulk nanostructured metals and alloys, Mater. Trans. 60 (2019) 1518–1532.

[16] F. Humphreys, G.S. Rohrer, et al., Recrystallization and Related Annealing Phenomena, Elsevier, 2004.

[17] S.L. Semiatin, J.C. Soper, I.M. Sukonnik, Short-time beta grain growth kinetics for a conventional titanium alloy, Acta Mater. 44 (1996) 1979–1986.

[18] R.E. Reed-Hill, Physical Metallurgy Principles, Van Nostrand, New York, 1973.

[19] G. Deng, T. Bhattacharjee, Y. Chong, et al., Influence of Fe addition in CP titanium on phase transformation, microstructure and mechanical properties during high pressure torsion, J. Alloys Compd. 822 (2020) 153604.

[20] R. Zheng, T. Bhattacharjee, S. Gao, et al., Change of deformation mechanisms leading to high strength and large ductility in mg-Zn-Zr-Ca alloy with fully recrystallized ultrafine grained microstructures, Sci. Rep. 9 (2019) 11702.

[21] S. Yoshida, T. Ikeuchi, T. Bhattacharjee, et al., Effect of elemental combination on friction stress and Hall-Petch relationship in face-centered cubic high / medium entropy alloys, Acta Mater. 171 (2019) 201–215.

[22] N. Tsuji, Ultrafine grained steels, Tetsu-to-Hagané 88 (2002) 359–369.

[23] N. Tsuji, Unique mechanical properties of nanostructured metals, J. Nanosci. Nanotechnol. 7 (2007) 3765–3770.

[24] T. Furuhara, S. Takagi, H. Watanabe, et al., Crystallography of grain boundary α precipitates in a β titanium alloy, Metall. Mater. Trans. A 27A (1996) 1635–1646.

[25] R. Shi, V. Dixit, H.L. Fraser, et al., Variant selection of grain boundary a by special prior β grain boundaries in titanium alloys, Acta Mater. 75 (2014) 156–166.

[26] E. Sarath Kumar Menon, H.I. Aaronson, "Black plate" formation in Ti-X alloys, Acta Metall. 10 (1986) 1963–1973.

[27] E. Sarath Kumar Menon, H.I. Aaronson, Interfacial structure of Widmanstatten plates in a Ti-Cr alloy, Acta Metall. 34 (1986) 1975–1981.

[28] Y. Tatsuzawa, T. Kunieda, H. Fujii, Continuous cooling transformation characteristics of Ti-5Al-2Fe-3Mo, Tetsu-to-Hagané 104 (2018) 235–241.

[29] D. Qiu, R. Shi, P. Zhao, et al., Effect of low-angle grain boundaries on morphology and variant selection of grain boundary allotriomorphs and Widmanstatten side-plates, Acta Mater. 112 (2016) 347–360.

[30] D. Bhattacharyya, G.B. Viswanathan, H.L. Fraser, Crystallographic and morphological relationships between β phase and the Widmanstatten and allotriomorphic α phase at special β grain boundaries in an α/β titanium alloy, Acta Mater. 55 (2007) 6765–6778.

[31] D. Qiu, Pengyang Zhao, Chen Shen, et al., Predicting grain boundary structure and energy in BCC metals by integrated atomistic and phase-field modeling, Acta Mater. 164 (2019) 799–809.

[32] T. Furuhara, J.M. Howe, H.I. Aaronson, Interphase boundary structures of intragranular proeutectoid α plates in a hypoeutectoid Ti-Cr alloy, Acta Metall. 39 (1991) 2873–2886.

[33] J.C. Williams, F.H. Froes, J.C. Chesnutt, et al., Development of High-Fracture Toughness Titanium Alloy, American Society for Testing and Materials 1978.

[34] Rebecca D. Dar, Haoxue Yan, Ying Chen, Grain boundary engineering of Co–Ni–Al, Cu–Zn–Al, and Cu–Al–Ni shape memory alloys by intergranular precipitation of a ductile solid solution phase, Scr. Mater. 115 (2016) 113–117.

[35] Y.T. Zhu, X.Z. Liao, Nanostructured metals retaining ductility, Nat. Mater. 3 (2004) 351–352.

[36] H.V. Swygenhoven, Grain boundaries and dislocations, Science 296 (2002) 66–67.

[37] V. Yamakov, D. Wolf, S.R. Phillpot, et al., Deformation-mechanism map for nanocrystalline metals by molecular-dynamics simulation, Nat. Mater. 3 (2004) 43–47.

[38] H.V. Swygenhoven, J.R. Weertman, Mechanical properties of fully dense nanocrystalline metals, Scr. Mater. 49 (2003) 625–627.

[39] R.A. Wood, R.J. Favor, Titanium Alloys Handbook. , Metals and Ceramics Information Center, 1972.